Resonant-Cavity-Enhanced Far-Infrared Upconversion Imaging Devices

L. K. Wu and W. Z. Shen

Abstract—We have carried out a detailed investigation on the application of resonant cavities to the photon-frequency-upconversion-based far-infrared (FIR) semiconductor imaging devices. The employment of a bottom mirror (BM) enhances the FIR photon absorption efficiency and, therefore, increases the quantum efficiency of GaAs homojunction interfacial work- function internal photoemission (HIWIP) FIR detectors. Significant improvement of the extraction efficiency could be achieved in resonant cavity enhanced (RCE) GaAs–AlGaAs near-infrared (NIR) light-emitting diodes (LEDs) through redirecting as many NIR photons as possible into the escape cone. Under the optimal structural parameters, we have predicted that the upconversion quantum efficiency of the integrated HIWIP-BM-RCE-LED imaging device could be boosted to 5–6 times of the normal HIWIP-LED upconverter without any resonant cavities. As a consequence of few reincarnation cycles needed by NIR photons to escape in the photon recycling process, we can further expect sharp and high-resolution imaging in HIWIP-BM-RCE-LED.

Index Terms—Cavity resonators, infrared imaging, optical frequency conversion, semiconductor device modeling.

I. INTRODUCTION

IN THE visible and near-infrared (NIR) region, the conventional silicon charged coupled devices (CCDs) are high performance and low cost image sensors with the detection wavelength up to about 1 μm. Beyond the Si CCD response range, the imaging of midinfrared (MIR) and far-infrared (FIR) radiation has a lot of applications, such as surveillance, tracking, biomedicine, space astronomy, quantum computing, and spectroscopy. Currently, the MIR imaging is often achieved by expensive InSb and HgCdTe arrays, while there are no semiconductor image sensors commercially available for the FIR radiation. The concept of the photon frequency upconversion proposed in 1960s [1] provides possibilities for semiconductor detection imaging of arbitrary wavelength light. By integrating a MIR/FIR semiconductor photodetector with a NIR light-emitting diode (LED) under a forward bias, one can expect the increase of the potential drop across the LED due to the reduction of the photodetector resistance upon MIR/FIR radiation. The upconverted image of the MIR/FIR object is realized by the short NIR emission from

the LED, which falls into the efficient imaging range of the Si CCD. Liu *et al.* [2], [3] have demonstrated successfully the MIR detection imaging with an upconverter consisting of a GaAs–AlGaAs quantum-well infrared photodetector (QWIP) and an In-GaAs–GaAs LED. The detection imaging of QWIP-LED [4], photon recycling effect in LED [5], and photonic breakdown in QWIP [6] have been further investigated theoretically in order to understand the MIR imaging mechanism and improve the performance of the QWIP-LED upconverter. We have proposed a FIR semiconductor upconversion device [7] through integrating a GaAs homojunction interfacial work-function internal photoemission (HIWIP) FIR detector [8] with a GaAs–AlGaAs NIR LED, and studied the imaging characteristics and quantum efficiency of the HIWIP-LED upconverter.

It should be noted that this kind of semiconductor upconverter is not necessarily separated into pixels with sufficient number of periodic structures in QWIP [2], [4] and HIWIP [7] under the condition of weak carrier lateral diffusion in the LED, since the output distribution of the photocurrent density driving the LED can almost reproduce the spatial distribution of the incident IR radiation intensity [4]. This avoids the conventional silicon readout circuit hybridization for detection imaging, and can bring down significantly the cost of IR imaging. However, the keys to practical application of these upconverter imaging devices are high quantum efficiency and good image quality. With the optimal parameters of the imaging systems, the QWIP-LED and HIWIP-LED upconversion devices could be pixelless with satisfying image quality [2], [4], [7]. Nevertheless, in the normal LED, the semiconductor refractive index is rather high, only those photons with the incident angle smaller than the critical angle θ_c could escape the LED due to the total internal reflection. Accordingly, the external efficiency of the LED is not high and the upconversion efficiency of the QWIP-LED MIR upconverter is very low (1%–3%) [9]. This could get even worse in the HIWIP-LED FIR upconverter due to the poor free carrier absorption efficiency of the GaAs HIWIP FIR detector, manifesting the upconversion efficiency of only ~1% [7].

To improve the performance of the semiconductor upconversion devices, a heterostructure bipolar transistor structure has been proposed into the QWIP-LED upconverter to amplify the photocurrent signal [10]. Another efficient way is to employ a resonant-cavity-enhanced LED (RCE-LED) [11], but without any detailed investigation until now. With an appropriate resonant cavity design, the preferential propagation direction of the NIR photons can be forced from total reflection regime toward the extraction cone [12], so the quantum efficiency of LED could be improved, and NIR photons need less number of reincarnations to emit out in the photon recycling [13]. Due to the long
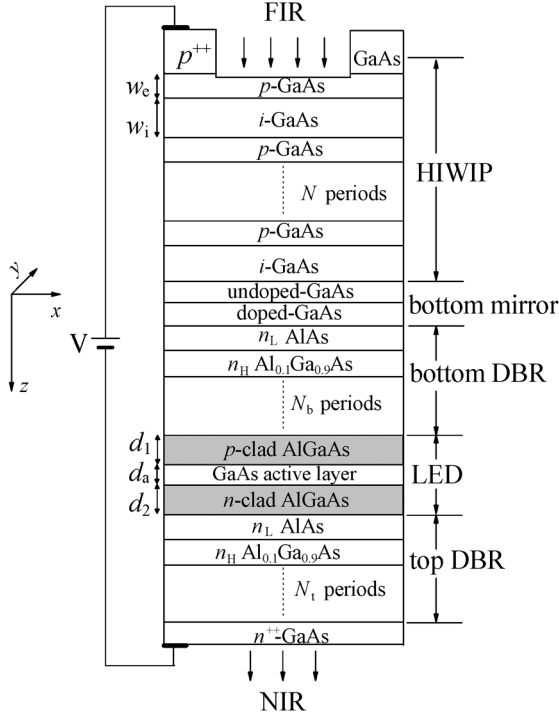
Fig. 1. Schematic view of the cross section of an integrated HIWIP-BM-RCE-LED FIR to NIR upconverter.

wavelength and free carrier absorption nature in the HIWIP FIR detector, the design of RCE HIWIP photodetectors is more complex in comparison with the NIR and MIR ones. Recently, we have demonstrated that the absorption efficiency could increase significantly in the GaAs HIWIP FIR detector with a single period of undoped/doped GaAs bottom mirror (BM) through the resonant absorption [14]. In the present work, we apply the resonant cavity structures to both the HIWIP FIR detector and NIR LED. We will show that the upconversion quantum efficiency of incoming FIR radiation to output NIR light can be boosted to 5–6 times in the HIWIP-BM-RCE-LED upconverters with even better NIR image quality of the FIR object, as compared with their HIWIP-LED counterparts.

II. THEORETICAL BACKGROUND

Fig. 1 shows the diagram of a HIWIP-BM-RCE-LED integrated upconversion imaging device and its operating principle under an applied bias V on the top p^{++}-GaAs and bottom n^{++}-GaAs contact layers. The basic structure of GaAs HIWIP FIR detector consists of several (N) periods of heavily doped p-GaAs emitter layers (thickness w_e) and undoped GaAs intrinsic layers (thickness w_i) across which most of the voltage is dropped. As stated in the Introduction, we employ a single period of undoped/doped GaAs BM with the reflectivity R_2 to realize the resonant absorption of the FIR photons [14], the top mirror of the detector resonant cavity can be the native semiconductor to air interface. The double heterostructure NIR LED consists of narrow-gap GaAs active layer bounded by two wide-gap confining p- and n-AlGaAs layers, with the thickness $d_a, d_1,$ and d_2, respectively. The N_t and N_b pairs of distributed Bragg reflector (DBR) serve as the top and bottom mirrors of the NIR RCE-LED. Considering the lattice matching, we

choose AlAs and $Al_{0.1}Ga_{0.9}$ As as the low (n_L) and high (n_H) refraction indexes of the DBR. We note that the existence of resonant cavities would not induce the obvious change in the electrical characteristics of the system [15], [16].

Under the nonuniform FIR radiation, the holes of the low energy states in the emitter layers of the GaAs HIWIP FIR detector are photoexcited to high energy ones, diffuse to the emitting interfaces and tunnel through the interfacial barriers determined by the bandgap narrowing effect, and then collected by the image force at the interfaces under a favorable applied forward bias [17]. The nonuniform photocurrent from the GaAs HIWIP FIR detector injects into the NIR LED active region. Confined by the p-clad and n-clad AlGaAs layers, most of the photocarriers recombine there and lead to nonuniform NIR radiation through the spontaneous radiative recombination, so the upconversion of FIR scenes to NIR images is realized.

We employ the spectral decomposition approach to analyze the performance of the HIWIP-BM-RCE-LED upconverter. The radiation photon flux distribution of a two-dimensional sine target is assumed $\phi^{in} = \phi_0^{in} + \phi_{\overrightarrow{f}}^{in} \cos 2\pi \overrightarrow{f} \overrightarrow{r}$, with $\overrightarrow{r} = (x, y), \phi_0^{in}$ the average photon flux of the incoming FIR radiation, f the spatial frequency, and $\phi_{\overrightarrow{f}}^{in}$ the signal part amplitude of the sine wave. Under the resonant condition, destructive interference occurs at the interfaces between emitter and intrinsic layers, and the reflection at the interfaces could be ignored. From a scalar-wave view in the detector resonant cavity, the forward traveling part of the incident FIR light wave electrical field at the top interface is the sum of the transmitted field and the feedback after a round trip in the cavity, the backward traveling part is the reflected wave of the FIR light at the bottom mirror [18]. We could calculate the light power absorbed in the detector resonant cavity through both the traveling parts. Neglecting the absorption in the intrinsic layers and considering the diffusion of holes in the active layers and collection at the interfaces, we have the ratio of photocarriers across the interfacial barriers between the emitter and intrinsic layers G [18]

$$G = \frac{[1 + R_2 \exp(-\alpha_p w_e)](1 - R_1)}{[1 - \sqrt{R_1 R_2} \exp(-\alpha_p w_e)]^2}$$
$$\times [1 - \exp(-\alpha_p w_e)] \exp\left(-\frac{w_e}{l}\right) \exp\left(-\frac{x_b}{l_s}\right) \quad (1)$$

here R_1 is the reflectivity of the top interface of the GaAs HIWIP FIR detector, R_2 is the reflectivity of the BM, α_p is the coefficient of free carrier absorption, $\alpha_p = 8.28 \times 10^{-16}$ cm$^2 \times N_a$ [8] with N_a the doping concentration of the p-GaAs emitter layers, x_b is the distance from the interface to the barrier maximum in the GaAs HIWIP FIR detector, and $l_s = 276 \pm 2$ Å [8] is the hole scattering length in the image force well. The first two terms on the right-hand side of (1) are associated with the photocarriers excited by the FIR absorption in the single emitter layer, the third term describes the carrier scattering loss during reaching the interface, and the last exponential indicates the capability of the carriers traveling from the interface to the barrier maximum due to the image force effect.

We neglect the impurity compensation in the p-GaAs emitter layers, the carrier diffusion along the axis z, and the carrier drift along axes x and y. By assuming that the in-plane potential is uniform within the emitter layers, we can write the output photocurrent density j from the current continuity equation of the hole transport in the HIWIP FIR detector [7]

$$j = j_0 + j_{\overrightarrow{f}} \cos 2\pi \overrightarrow{f} \overrightarrow{r} \tag{2a}$$

with the average photocurrent density j_0 of

$$j_0 = \frac{qG\phi_0^{\text{in}}}{p_c} \tag{2b}$$

and the signal part amplitude of the output current density $j_{\overrightarrow{f}}$ of

$$j_{\overrightarrow{f}} = qG\phi_{\overrightarrow{f}}^{\text{in}} \exp(-4\pi^2 l^2 f^2)$$
$$\times \frac{1 - (1 - p_c)^N \exp(-4\pi^2 l^2 f^2 N)}{1 - (1 - p_c) \exp(-4\pi^2 l^2 f^2)} \tag{2c}$$

where q is the unit charge, p_c is the capture probability [19] of holes in the GaAs emitter layers, and l is the characteristic diffusion length. The inverse relationship of p_c and j_0 in (2b) is due to the fact that more photocarriers will be captured during the transport for larger p_c, resulting in the smaller generation of j_0.

In the commonplace LED, the small critical cone angle imposed by Snell's law covers a solid angle of only $\approx (1/4n^2) \times 4\pi$ steradians, resulting in a low extraction efficiency η^{pc} of photons. Take GaAs–AlGaAs NIR LED for example, since the refractive index n of GaAs is high (~ 3.527), the extraction efficiency is only $\sim 2\%$. It has been demonstrated that the photon recycling mechanism in high-quality LED could improve the quantum efficiency, emitted photons undergoes as many reabsorption and reemission cycles as necessary in the active layer until a favorable angle is found, while at the same time, the NIR photons will experience parasitic losses and nonradiative losses in the cycles [13]. The DBR cavity strongly enhances the extraction probability of photons and reduces the average number of cycles in the photon recycling before a NIR photon escapes, relieving the high-quality material demand of LED for far more practical device design.

We can examine the extraction efficiency η^{pc} of the NIR RCE-LED via the method proposed by Benisty *et al.* [12], [20]. In the DBR resonator, the spontaneous emission of electron–hole pairs can adequately be represented by an electric dipole. Decomposing an arbitrary linear polarization of the dipoles in NIR RCE-LED into transverse electric [s, only for horizontal (h) dipoles] and transverse magnetic [p, for both horizontal and vertical (v) ones] [20], we get the emitted intensity $I^{\text{or,pol}}(\theta)$ (or $= h, v$; pol $= s, p$)

$$I^{\text{or,pol}}(\theta) = (1 - r_1^2)|A^{\text{or,pol}}|^2|1 + r_2 \exp(2i\varphi')|^2$$
$$\times |1 - r_1 r_2 \exp(2i\varphi)|^2 \tag{3}$$

with θ the internal emission angle of dipoles, r_1 (r_2) the top (bottom) amplitude reflection, $A^{\text{or,pol}}$ the source terms of different dipoles [21], $2\varphi' = 2\beta k l_c \cos(\theta) + p_2$, and

$2\varphi = 2k l_c \cos(\theta) + p_1 + p_2$, where $l_c = d_1 + d_2$ (in the real structure of RCE-LED, the thickness of the active layer d_a is much less than the length of the cavity l_c [22] and could be neglected here), $\beta = d_1/l_c$ is the source position, k is the wavevector, p_1 and p_2 are the phase shifts of the NIR radiation reflecting on the top and bottom DBRs, respectively. For bulk semiconductor material where the emitting dipoles are isotropic on average, the total emitted angular intensity $I(\theta)$ is given by [20]

$$I(\theta) = \frac{2}{3}[I^{h,s}(\theta) + I^{h,p}(\theta)] + \frac{1}{3}I^{v,p}(\theta) \tag{4}$$

and η^{pc} of the NIR RCE-LED can be obtained via

$$\eta^{\text{pc}} = \frac{2\pi \int_0^{\theta_c} I(\theta)\sin(\theta)d\theta}{2\pi \int_0^{\frac{\pi}{2}} I(\theta)\sin(\theta)d\theta}. \tag{5}$$

In RCE-LED, the Purcell factor is close to one, resulting in a negligible spontaneous emission rate enhancement [20]. The spatial photon flux distribution of the output NIR radiation from the NIR RCE-LED is

$$\phi^{\text{out}} = \eta^{\text{pc}} \frac{\sum(x)}{\tau_r} \tag{6}$$

where $\sum(x)$ and τ_r are the sheet concentration and radiative recombination lifetime of the injected photocarriers in the active region, respectively. Under the condition of photon recycling effect, the sheet concentration $\sum(x)$ is related with the output photocurrent density j and the fluxes of the NIR radiation propagating back and forth ($\phi_{\pm}^{\text{out}}$) along the active region [5]

$$-D\frac{d^2\sum(x)}{dx^2} + \left(\frac{1}{\tau_r} + \frac{1}{\tau_n}\right)\sum(x) = \frac{j}{q} + v_g\alpha_1(\phi_+^{\text{out}} + \phi_-^{\text{out}}) \tag{7a}$$

$$\pm\frac{d\phi_{\pm}^{\text{out}}}{dx} + \alpha_2\phi_{\pm}^{\text{out}} = \frac{(1 - \eta^{\text{pc}})}{2v_g}\frac{\sum(x)}{\tau_r} \tag{7b}$$

where D and τ_n are the diffusion coefficient and nonradiative lifetime of the injected photocarriers in the active layer, respectively, v_g is the photon group velocity, $\alpha_1 = \alpha_a\Gamma$, $\alpha_2 = \alpha_a\Gamma + \alpha_c(1 - \Gamma)$, where α_a is the photon absorption coefficient for the active region, α_c is that for the surrounding layers, and $\Gamma = d_a/(d_a + d_1 + d_2)$.

By solving the (6) and (7), we have the output NIR photon flux

$$\phi^{\text{out}} = \phi_0^{\text{out}} + \phi_{\overrightarrow{f}}^{\text{out}} \cos 2\pi \overrightarrow{f} \overrightarrow{r} \tag{8a}$$

with the average photon flux ϕ_0^{out} of

$$\phi_0^{\text{out}} = \frac{\eta^{\text{pc}}\eta_{\text{int}}j_0}{q\left[1 - (1 - \eta^{\text{pc}})\left(\frac{\alpha_1}{\alpha_2}\right)\eta_{\text{int}}\right]} \tag{8b}$$

and the signal part amplitude $\phi_{\overrightarrow{f}}^{\text{out}}$ of

$$\phi_{\overrightarrow{f}}^{\text{out}} = \frac{\eta^{\text{pc}}\eta_{\text{int}}j_{\overrightarrow{f}}}{q\left[1 + 4\pi^2 f^2 l_d^2 - (1 - \eta^{\text{pc}})\left(\frac{\alpha_1\alpha_2}{\alpha_2^2 + 4\pi^2 f^2}\right)\eta_{\text{int}}\right]} \tag{8c}$$

where l_d is the diffusion length of carriers in the GaAs active layer, and η_{int} is the internal quantum efficiency of the NIR RCE-LED: $\eta_{\text{int}} = \tau_n/(\tau_n + \tau_r)$.

III. QUANTUM EFFICIENCY OF HIWIP-BM

The free carrier absorption in the emitter layers will be intensified after adding a bottom mirror to the GaAs HIWIP FIR detector, which benefits to the quantum efficiency $\eta^{\text{HIWIP−BM}}(f)$ of the HIWIP-BM structures. Using (1) and (2), we can obtain, under the resonant condition,

$$
\begin{aligned}
\eta^{\text{HIWIP−BM}}(f) = \frac{j_{\overline{f}}/q}{\phi_{\overline{f}}^{\text{in}}} &= \frac{[1 + R_2 \exp(-\alpha_p w_e)](1 - R_1)}{[1 - \sqrt{R_1 R_2} \exp(-\alpha_p w_e)]^2} \\
&\times \frac{1 - (1 - p_c)^N \exp(-4\pi^2 l^2 f^2 N)}{1 - (1 - p_c) \exp(-4\pi^2 l^2 f^2)} \\
&\times [1 - \exp(-\alpha_p w_e)] \exp(-4\pi^2 l^2 f^2) \\
&\times \exp\left(-\frac{w_e}{l}\right) \exp\left(-\frac{x_b}{l_s}\right)
\end{aligned}
\tag{9}
$$

where $\exp(-w_e/l)$ is the internal photoemission efficiency indicating the probability of the photoexcited carriers reaching the p-GaAs–i-GaAs interface by diffusion, $\exp(-x_b/l_s)$ is the barrier collection efficiency, and the other part on the right-hand side of (9) is the photon absorption efficiency, which represents the detector cavity enhancement effect. The top of the FIR detector cavity is the native semiconductor and air interface, the large refractive index difference at the boundary provides a reflectivity of $R_1 \approx 30\%$ [18]. Due to the long wavelength of FIR radiation, the normal DBR cannot provide effective reflectivity, and one-fourth wavelength of the thickness is beyond the ability for the molecular beam epitaxy growth of the integrating upconverter structures. We have demonstrated the powerful undoped/doped GaAs bottom mirrors for FIR reflection [14].

Except for the following examined parameters, the relationship between the other parameters of GaAs FIR HIWIP-BM detectors and $\eta^{\text{HIWIP−BM}}(f)$ is the same as the case of the normal FIR detectors without bottom mirrors, so the other parameters selected in the calculations comply fully with [7]. We study the dependences of $\eta^{\text{HIWIP−BM}}(f)$ on w_e, R_2, and N_a at a characteristic spatial frequency $f = 5$ lp/mm, as shown in Fig. 2. From Fig. 2(a), we can observe that $\eta^{\text{HIWIP−BM}}(f)$ increases with R_2 at any w_e. This is due to the fact that with the larger R_2, more FIR radiation is reflected back by the bottom mirror and the absorption in the emitter layers is enhanced. However, $\eta^{\text{HIWIP−BM}}(f)$ exhibits a maximum at a certain w_e of ∼40 nm, different from the optimal w_e (≈20 nm) for the normal GaAs HIWIP FIR detector [7]. With the increase of emitter layer thickness w_e, the photon absorption efficiency will increase, while the internal photoemission efficiency decreases. Due to the bottom mirror effect, the photon absorption efficiency dominates $\eta^{\text{HIWIP−BM}}(f)$ at small w_e, resulting in the increase of $\eta^{\text{HIWIP−BM}}(f)$ with w_e. Further increase of w_e will lead to the rapid decrease of the internal photoemission efficiency, and, therefore, the decrease of $\eta^{\text{HIWIP−BM}}(f)$. The involvement of the bottom mirror will modify the optimal w_e for maximal quantum efficiency.

It should be noted that the present quantum efficiencies are consistent with the previous results under resonant condi-
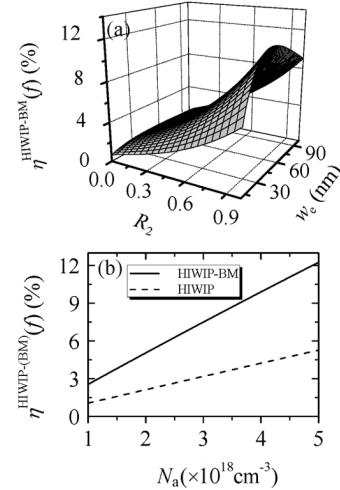

Fig. 2. (a) Calculated quantum efficiency of the HIWIP-BM FIR detector vs the reflectivity of the bottom mirror R_2 and the emitter layer thickness w_e under $N_a = 4.0 \times 10^{18}$ cm^{-3}, $p_c = 0.07$, and $f = 5$ lp/mm. (b) Dependence of the quantum efficiency of the HIWIP-(BM) FIR detector on the emitter layer doped concentration N_a at $w_e = 40$ nm, $p_c = 0.07$, $R_2 = 0.9$, and $f = 5$ lp/mm.

tion [23] after considering approximately 35% of the barrier collection efficiency with the optimal parameters. The FIR radiation absorption efficiencies also agree well with those obtained through the transfer matrix method [24]. Fig. 2(b) presents the effect of the emitter layer concentration N_a on the quantum efficiency of the GaAs HIWIP FIR detector with and without the bottom mirror. We note that the larger N_a is, the more carriers can be photoexcited, and $\eta^{\text{HIWIP−(BM)}}(f)$ is proportional to N_a no matter whether there is a bottom mirror in the HIWIP FIR detector. However, N_a cannot be increased indefinitely, it is limited by the Mott transition concentration (≈5.02×10^{18} cm^{-3} for p-GaAs [17]), under which our HIWIP FIR detectors cannot work. Here we choose $N_a = 4.0 \times 10^{18}$ cm^{-3} for the FIR detection wavelength centered at 60 μm, the same as the value in the case of normal HIWIP-LED [7]. Furthermore, it is clear from Fig. 2(b) that we can achieve large improvement (more than two times of the common FIR HIWIP case at 4.0×10^{18} cm^{-3}) of the quantum efficiency in GaAs FIR detectors with resonant bottom mirrors. This is expectable since the photon absorption will be enhanced dramatically with a small increase of N_a there.

IV. QUANTUM EFFICIENCY OF RCE-LED

The application of DBR cavity to the NIR LED is helpful for the improvement of the extraction efficiency η^{pc}. Due to the large absorption coefficient of GaAs at the LED emission wavelength, we select the typical AlAs–Al$_{0.1}$Ga$_{0.9}$As DBR for the NIR LED, instead of the AlAs–GaAs one, with the low refractive index of AlAs ($n_L = 2.970$), the high one of Al$_{0.1}$Ga$_{0.9}$As ($n_H = 3.527$), and the resonant wavelength of 0.88 μm, which falls into the efficient imaging range of conventional Si CCDs. Here, we employ the hard mirror approximation [25] of a reflector with a constant complex reflectivity r for the DBR

$$
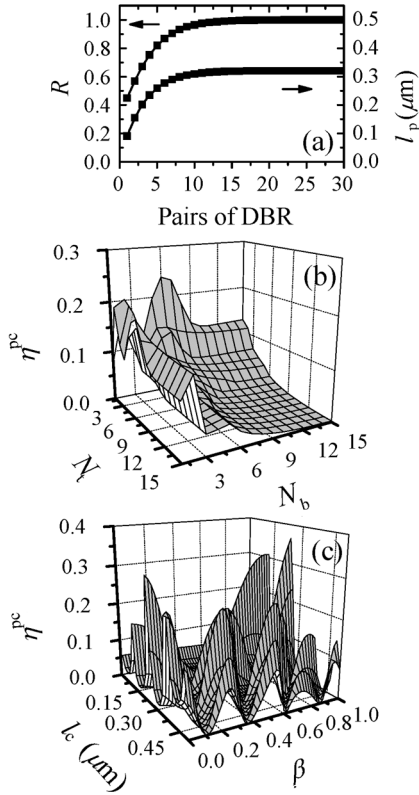r = r_c \exp[-2i(k - k_z)l_p]
\tag{10}
$$

Fig. 3. (a) Reflectivity R and penetration length l_p of the DBR as a function of number of DBR pairs. The relationship of the NIR RCE-LED extraction efficiency η^{pc} with (b) the number of top DBR pairs N_t and bottom DBR pairs N_b under $l_c = 0.25\ \mu\mathrm{m}$ and $\beta = 0.9$, and (c) the DBR cavity length l_c and source position β at $N_t = 1$ and $N_b = 6$.

where r_c is the amplitude reflectivity of the DBR, $k_z = k\cos(\theta)$, and l_p is the penetration length of the NIR photons, which is proportional to the phase shift of the NIR radiation reflecting on the DBR. r_c and l_p depend on the number of DBR pairs (including both the top and bottom DBRs) [25], and Fig. 3(a) has displayed the calculated relationships between the power reflectivity $R(= r_c^2)$, l_p and the number of DBR pairs. It is seen that both R and l_p first increase with the number of DBR pairs, and then saturate (R to unit and l_p to a certain value) when the top and bottom DBRs have more than 13 pairs.

With the top and bottom DBRs in the NIR LED, the interference effects will lead to the modification of the internal angular power distribution. The propagation direction of NIR photons would have a large probability to fall into the critical angle, i.e., the enhancement of η^{pc}. As a result, it is important to optimize the top and bottom DBR mirrors. Fig. 3(b) displays the effects of the number of top DBR pairs N_t and that of bottom DBR pairs N_b on the extraction efficiency η^{pc}. At small values of N_t and N_b, the interferences in the DBR cavity are diminished since the reflectivity of the top and bottom DBR mirrors is very low [see Fig. 3(a)], so high η^{pc} is hardly achieved. With large number of the DBR pairs, due to the significant phase shift of NIR light reflecting on DBRs [also see Fig. 3(a)], the cavity order (number of resonances, depends on the round-trip phase evolution of the NIR light in the DBR cavity) of NIR RCE-LED is high, which is adverse to η^{pc} [12]. The optimal number of DBR pairs should be a tradeoff between the high reflectivity and small phase shift of the NIR light. Furthermore, to ensure escape of the NIR photons

on the top side, the bottom mirror should be far more reflective than the top one [12], [22]. Based on the results in Fig. 3(b), we choose $N_t = 1$ and $N_b = 6$ as suitable numbers of the top and bottom DBR pairs.

In addition to the DBRs, the position of the active layer in NIR RCE-LED also plays important roles in the spatial distribution of the optical field. The standing wave effect indicates that the radiated emission in a particular direction is high if the standing wave field is strong at the source position, which can be utilized to enhance the emission within the critical angle of the NIR photons [20]. Fig. 3(c) exhibits vibrational behavior of η^{pc} with both source position (β) and cavity length (l_c). Considering the practical device design [22], we investigate the variation of η^{pc} with the cavity length l_c in the range of less than 0.5 μm. For very small values of l_c, the confinement of the n-clad and p-clad layers is weak and the carriers cannot recombine efficiently in the active layer, which leads to a low η^{pc}. In the large l_c range, the β dependence of η^{pc} indicates that, under a fixed l_c, we could obtain large η^{pc} when the active layer lies at certain positions of the cavity (where the standing wave effect is notable). Generally, η^{pc} can reach above 20%, consistent with the experimental result of $\eta^{\mathrm{pc}} \approx 22.8\%$ [26]. In the case of $l_c \approx 0.25\ \mu$m, we can expect a maximal η^{pc} when $\beta = 1$. However, $\beta = 1$ means that the n-clad layer does not exist and the buffering effect is absent, so we select $l_c = 0.25\ \mu$m and $\beta = 0.9$ as two optimal structural parameters of the NIR RCE-LED.

With the above optimal parameters, the extraction efficiency of the NIR RCE-LED can be achieved as high as 25%, more than 10 times of ~2% in normal NIR LED without the DBR cavity, showing significant enhancement of the extraction efficiency in NIR LED with DBRs. However, besides the extraction efficiency η^{pc}, the photon recycling effect [27] also plays an important role in the external quantum efficiency of RCE-LED $\eta^{\mathrm{RCE-LED}}(f)$, as revealed in [7]. The external quantum efficiency of the NIR RCE-LED under the photon recycling can be easily obtained from (8c)

$$\eta^{\mathrm{RCE-LED}}(f) = \frac{\phi_{\vec{f}}^{\mathrm{out}}}{j_{\vec{f}}/q}$$
$$= \frac{\eta^{\mathrm{pc}}\eta_{\mathrm{int}}}{1 + 4\pi^2 l_d^2 f^2 - (1-\eta^{\mathrm{pc}})\eta_{\mathrm{int}}\left(\frac{\alpha_1\alpha_2}{\alpha_2^2 + 4\pi^2 f^2}\right)}.$$
(11)

If we neglect the absorption in the confinement layers at small spatial frequencies, (11) reduces to $(\eta^{\mathrm{pc}}\eta_{\mathrm{int}})/[1-(1-\eta^{\mathrm{pc}})\eta_{\mathrm{int}}]$, the same expression as the quantum efficiency of RCE-LEDs taking into account the photon recycling effect in [28].

Within a DBR cavity, the photon recycling in LED could be changed due to the enhancement of the extraction efficiency. Furthermore, the absorption of NIR photons in the LED also depends on the thickness of the active layer, which in turn influences the photon recycling too. Fig. 4 presents the dependence of $\eta^{\mathrm{RCE-LED}}(f)$ on the LED active layer thickness d_a under different extraction efficiencies η^{pc} at a fixed spatial frequency of $f = 5$ lp/mm, together with the normal NIR LED with photon recycling for comparison. The increase of d_a intensifies the NIR photon absorption in the active layer and the trapped photons can be reabsorbed more efficiently, leading to the enhancement
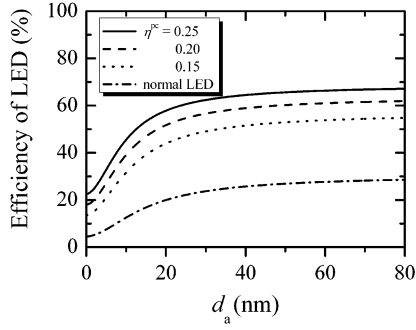
Fig. 4. Active layer thickness d_a dependence of RCE-LED external quantum efficiency at different η^{pc}, together with the normal LED case for comparison at $\eta_{\mathrm{int}} = 0.9$ and $f = 5$ lp/mm.

of photon recycling and a large $\eta^{\mathrm{RCE-LED}}(f)$. However, the nonradiative recombination of the injected photocarriers in the active layer will also increase with d_a, which limits the internal efficiency η_{int} [29], therefore $\eta^{\mathrm{RCE-LED}}(f)$ gradually saturates at $d_a = 30$ nm. The higher extraction efficiency induces fewer cycles needed by NIR photons to escape in the photon recycling process, the total optical parasitic optical losses and nonradiative recombination loss in the photon recycling are smaller [13], resulting in a higher external quantum efficiency of the NIR RCE-LED. Nevertheless, it should be pointed out that, due to the different photon recycling effects, although the extraction efficiency in RCE-LEDs can be enhanced more than ten times of normal LEDs, the comparison in Fig. 4 reveals only 2–3 times of the increase in the external quantum efficiency of RCE-LEDs over normal LEDs [7].

V. PERFORMANCE OF HIWIP-BM-RCE-LED

After demonstrating the improvement of the quantum efficiency in individual HIWIP FIR detector and NIR LED structures with the employment of resonant cavities, we further investigate the upconversion quantum efficiency $\eta(f)$ of the integrated HIWIP-BM-RCE-LED upconverter to see the efficiency of these two resonant cavities in converting the FIR radiation into the output NIR images. $\eta(f)$ is defined as $\eta(f) = \phi_{\overrightarrow{f}}^{\mathrm{out}}/\phi_{\overrightarrow{f}}^{\mathrm{in}}$ and can be easily yielded from (2c) and (8c). Fig. 5(a) shows the integrated HIWIP-BM-RCE-LED upconversion quantum efficiency $\eta(f)$ at different spatial frequencies f, together with $\eta(f)$ of the HIWIP-LED (without any resonant cavities) and HIWIP-BM-LED (without the resonant cavity in LED) for comparison. Clearly, the FIR radiation can be upconverted with different efficiencies at different f, and generally $\eta(f)$ is high for the large scale of image (small f), while low for the small size of image (large f). The employment of the two resonant cavities in the present integrated HIWIP-BM-RCE-LED structure has yielded a remarkable increase of the upconversion quantum efficiency to $\sim 6\%$, in contrast to that of $\sim 1\%$ in the HIWIP-LED and $\sim 2\%$ in the HIWIP-BM-LED ones: Each resonant cavity can improve the upconversion quantum efficiency 2–3 times.

In addition to the quantum efficiency, the image quality is another key specification for the performance of semiconductor upconversion devices. With the introduction of resonant cavi-
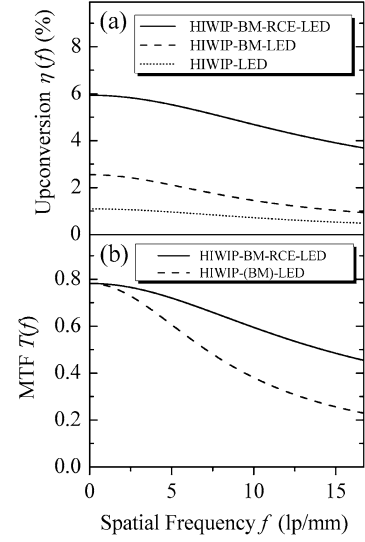

Fig. 5. Spatial frequency f dependence of (a) upconversion efficiency $\eta(f)$ and (b) modulation transfer function $T(f)$ of HIWIP-BM-RCE-LED and HIWIP-(BM)-LED at $p_c = 0.07$, $\eta_{\mathrm{int}} = 0.9$, and $d_a = 30$ nm.

ties, one may doubt whether the enhancement of upconversion quantum efficiency is at the sacrifice of good image quality? In order to investigate the imaging characteristics of the integrated HIWIP-BM-RCE-LED upconverter, we study the modulation transfer function (MTF) of the system, which is the ratio of the image contrast $(\phi_{\overrightarrow{f}}^{\mathrm{out}}/\phi_0^{\mathrm{out}})$ to the object contrast $(\phi_{\overrightarrow{f}}^{\mathrm{in}}/\phi_0^{\mathrm{in}})$ at different spatial frequencies f and can serve as the figure of merit of the imaging device [5]. The MTF $T(f)$ of the HIWIP-BM-RCE-LED upconverter can be yielded from (2b), (2c), (8b), and (8c)

$$
\begin{aligned}
T(f) = \frac{\phi_{\overrightarrow{f}}^{\mathrm{out}}/\phi_0^{\mathrm{out}}}{\phi_{\overrightarrow{f}}^{\mathrm{in}}/\phi_0^{\mathrm{in}}} &= p_c \exp\left(-4\pi^2 l^2 f^2\right) \\
&\times \frac{1 - (1-p_c)^N \exp(-4\pi^2 l^2 f^2 N)}{1 - (1-p_c)\exp(-4\pi^2 l^2 f^2)} \\
&\times \frac{1 - (1-\eta^{\mathrm{pc}})\eta_{\mathrm{int}}\left(\frac{\alpha_1}{\alpha_2}\right)}{1 + 4\pi^2 l_d^2 f^2 - (1-\eta^{\mathrm{pc}})\eta_{\mathrm{int}}\left(\frac{\alpha_1\alpha_2}{\alpha_2^2 + 4\pi^2 f^2}\right)}. \quad (12)
\end{aligned}
$$

Due to the diffraction limit, only images with $f \leqslant f_{\lambda_{\mathrm{in}}} = 1/\lambda_{\mathrm{in}} \approx 16.7$ lp/mm can be resolved (λ_{in} is the wavelength of the incoming FIR light, and we have selected 60 μm as the center detection wavelength in the present study). Although the absorption of FIR photons in the emitter layers intensifies by applying a BM to the GaAs HIWIP FIR detector, the proportion of the nonuniform photocurrent $j_{\overrightarrow{f}}$ to the uniform one j_0 keeps the same [see (2b) and (2c)], resulting in the unchanged ratio of the signal NIR photon flux to the average part. Therefore, the image contrast will not be affected by the BM, and the image quality of the HIWIP-BM-LED is the same as that of HIWIP-LED.

Fig. 5(b) presents the comparison of the MTF curves between HIWIP-BM-RCE-LED and HIWIP-(BM)-LED at different spatial frequencies. Sandwiched by two DBR mirrors, the extrac-

tion efficiency η^{pc} of NIR RCE-LED has increased, leading to less number of reincarnation cycles needed by the NIR photon before it emits out. Take $\eta^{\mathrm{pc}} = 25\%$ for instance, according to the analysis of photon recycling effect in LED [13], if there is no parasitic optical losses and the internal quantum efficiency of NIR RCE-LED is high enough, the NIR photons will experience 4 reincarnation cycles on average to escape. Since the diffusion length l_{d} of photocarriers in the NIR LED is about 1 μm [7], the total diffusion length in the NIR RCE-LED with the 25% extraction efficiency is about 4 μm, less than the smallest nonuniformity limited by diffraction ($1/2\pi f_{\lambda_{\mathrm{in}}} \approx 9.6\,\mu$m). As a result, the DBR cavity could reduce the image smearing, and we do observe much higher MTF $T(f)$ in HIWIP-BM-RCE-LED, compared with that of HIWIP-(BM)-LED, in the whole range of spatial frequency studied. Furthermore, $T(f)/T(0)$ is always larger than 0.5 in HIWIP-BM-RCE-LED, indicating that the imaging there will have perceived sharpness and resolution even in size of details. The above arguments of much higher upconversion quantum efficiency and better image quality reveal clearly the role of resonant cavities in semiconductor upconverters of FIR imaging.

Finally, we discuss the possible crosstalk resulting from the leaked NIR signal from the LED absorbed by the GaAs layer of the FIR detector. The electrons and holes generated by the leaked NIR light will change the charges in the emitter layers and result in an additional redistribution of the electric field across the FIR detector, which contributes to the detector photocurrent feeding the LED. Under the condition of large photoconductive gain, the "gained photocurrent" associated with the NIR light reabsorption in the FIR detector can lead to a diverging rise of the NIR output light, i.e., the photonic breakdown phenomenon [6]. The photonic breakdown will result in an increase of the uniform portion in the output NIR radiation, in comparison with the nonuniform (image signal) part, which induces the deterioration of the image quality.

However, in our HIWIP-BM-RCE-LED upconversion structure, once a NIR photon is generated in LED, it may have one of following four possible destinies: 1) it can emit out through the escape cone determined by the internal total reflection; 2) it can be reabsorbed in the active layer and experience reincarnation as a NIR photon (the photon recycling effect); 3) it can be reabsorbed by the parasitic optical losses in the structure during the photon recycling, or may lose in the nonradiative recombination processes; and 4) it would emit towards the bottom DBRs of the LED and might have a small probability to pass through the DBRs and propagate over the HIWIP FIR detector. It is obvious that those NIR photons belonging to possibilities 1)–3) would not be absorbed by the GaAs emitter layer of the FIR detector, only the possibility 4) of the NIR photons may contribute to the reabsorption by the FIR detector. Furthermore, due to the high reflectivity of the bottom DBRs for the LED [We have selected 6 DBR pairs as the bottom DBR mirror, the reflectivity of which may be as high as 85%, as shown in Fig. 3(a)], irrespective of the DBR absorption losses, only 15% of the possibility 4) NIR photons at most could penetrate through the bottom DBR mirror and be absorbed by the FIR detector. Therefore, the leaked NIR photons from the LED are negligible comparing with the total NIR photons generated in the LED. In addition, the bias under which the FIR detector works is around 200 mV, i.e., the electric field (2–4×10^2 V/cm) is lower as compared with the photonic breakdown field of $> 10^3$ V/cm. As a result, the crosstalk phenomenon between the LED and the FIR detector can be negligible in our HIWIP-BM-RCE-LED upconverter.

VI. Conclusion

We have predicted by theoretical simulations that the quantum efficiency of the HIWIP-LED upconverter could be greatly improved via the employment of BM for the GaAs HIWIP FIR detector and DBR cavity for the NIR LED. With the optimal device parameters, the upconversion quantum efficiency of HIWIP-BM-RCE-LED could have a large increase of 5–6 times and the image quality is even better, in comparison with those of the normal HIWIP-LED without any resonant cavities. It is the enhancement of the FIR photon absorption in the emitter layers that leads to a high quantum efficiency of the HIWIP-BM FIR detector, with the same image transfer due to the unchanged image contrast. The investigation of the NIR RCE-LED indicates that the resonant DBR cavity improves significantly the extraction efficiency of the LED with a high-index active layer, through redirecting as many NIR photons as possible into the escape cone by means of interferences. Though the photon recycling effect is not as effective as the normal LED in the enhancement of the LED quantum efficiency, we still could expect much increased external quantum efficiency in the NIR RCE-LED. Furthermore, as a consequence of few reincarnation cycles needed by NIR photons to escape in the photon recycling process, the diffusion of photocarriers is weak in the active layer of the NIR RCE-LED, resulting in sharp and high-resolution imaging in HIWIP-BM-RCE-LED. The present achievement in both the upconversion quantum efficiency and image characteristics opens the way to experimental realization of the FIR radiation upconversion imaging by the HIWIP-BM-RCE-LED upconverter.

References

[1] P. W. Kruse, F. C. Pribble, and R. G. Schulze, "Solid-state infrared-wavelength converter employing high-quantum-efficiency Ge-GaAs heterojunction," *J. Appl. Phys.*, vol. 38, no. 4, pp. 1718–1720, Mar. 1967.

[2] H. C. Liu, J. Li, Z. R. Wasilewski, and M. Buchanan, "Integrated quantum well intersub-band photodetector and light emitting diode," *Electron. Lett.*, vol. 31, no. 10, pp. 832–833, May 1995.

[3] L. B. Allard, H. C. Liu, M. Buchanan, and Z. R. Wasilewski, "Pixelless infrared imaging utilizing a p-type quantum well infrared photodetector integrated with a light emitting diode," *Appl. Phys. Lett.*, vol. 70, no. 1, pp. 2784–2786, Mar. 1997.

[4] V. Ryzhii, H. C. Liu, I. Khmyrova, and M. Ryzhii, "Analysis of integrated quantum-well infrared photodetector and light-emitting diode for implementing pixelless imaging devices," *IEEE J. Quantum Electron.*, vol. 33, no. 9, pp. 1527–1531, Sep. 1997.

[5] V. Ryzhii, I. Khmyrova, and P. Bois, "Photon mechanism of image smearing in integrated QWIP-LED pixelless devices," *IEEE J. Quantum Electron.*, vol. 35, no. 11, pp. 1693–1696, Nov. 1999.

[6] V. Ryzhii and H. C. Liu, "Photonic breakdown in up-conversion imaging devices based on the integration of quantum-well infrared photodetector and light-emitting diode," *J. Appl. Phys.*, vol. 92, no. 5, pp. 2354–2358, Sep. 2002.

[7] L. K. Wu and W. Z. Shen, "Far-infrared upconversion imaging devices: Imaging characteristics and quantum efficiency," *J. Appl. Phys.*, vol. 100, p. 044508-(1–6), Aug. 2006.

[8] W. Z. Shen, A. G. U. Perera, H. C. Liu, M. Buchanan, and W. J. Schaff, "Bias effects in high performance GaAs homojunction far-infrared detectors," *Appl. Phys. Lett.*, vol. 71, no. 18, pp. 2677–2679, Nov. 1997.

[9] E. Dupont, M. Byloos, M. Gao, M. Buchanan, C.-Y. Song, Z. R. Wasilewski, and H. C. Liu, "Pixelless thermal imaging with integrated quantum-well infrared photodetector and light-emitting diode," *IEEE Photon. Technol. Lett.*, vol. 14, no. 2, pp. 182–184, Feb. 2002.

[10] S. Oktyabrsky, I. Khmyrova, and V. Ryzhii, "Characteristics of integrated QWIP-HBT-LED upconverter," *IEEE Trans. Electron Devices*, vol. 50, no. 12, pp. 2378–2387, Dec. 2003.

[11] D. Ban, H. Luo, H. C. Liu, A. J. SpringThorpe, R. Glew, Z. R. Wasilewski, and M. Buchanan, "1.5 to 0.87 μm optical upconversion device fabricated by wafer fusion," *Electron. Lett.*, vol. 39, no. 15, pp. 1145–1147, Jul. 2003.

[12] H. Benisty, H. De Neve, and C. Weisbuch, "Impact of planar microcavity effects on light extraction—Part I: Basic concepts and analytical trends," *IEEE J. Quantum Electron.*, vol. 34, no. 9, pp. 1612–1631, Sep. 1998.

[13] I. Schnitzer, E. Yablonovitch, C. Caneau, and T. J. Gmitter, "Ultrahigh spontaneous emission quantum efficiency, 99.7% internally and 72% externally, from AlGaAs/GaAs/AlGaAs double heterostructures," *Appl. Phys. Lett.*, vol. 62, no. 2, pp. 131–133, Jan. 1993.

[14] Y. H. Zhang, H. T. Luo, and W. Z. Shen, "Demonstration of bottom mirrors for resonant-cavity-enhanced GaAs homojunction far-infrared detectors," *Appl. Phys. Lett.*, vol. 82, no. 7, pp. 1129–1131, Feb. 2003.

[15] D. W. Winston and R. E. Hayes, "Optoelectronic device simulation of bragg reflectors and their influence on surface-emitting laser characteristics," *IEEE J. Quantum Electron.*, vol. 34, no. 4, pp. 707–715, Apr. 1998.

[16] J. M. Fastenau and G. Y. Robinson, "Low-resistance visible wavelength distributed bragg reflectors using small energy band offset heterojunctions," *Appl. Phys. Lett.*, vol. 74, no. 25, pp. 3758–3760, Jun. 1999.

[17] A. G. U. Perera, H. X. Yuan, and M. H. Francombe, "Homojunction internal photoemission far-infrared detectors: Photoresponse performance analysis," *J. Appl. Phys.*, vol. 77, no. 2, pp. 915–924, Jan. 1995.

[18] M. S. Ünlü and S. Strite, "Resonant cavity enhanced photonic devices," *J. Appl. Phys.*, vol. 78, no. 2, pp. 607–639, Jul. 1995.

[19] W. Z. Shen and A. G. U. Perera, "Photoconductive generation mechanism and gain in internal photoemission infrared detectors," *J. Appl. Phys.*, vol. 83, no. 7, pp. 3923–3925, Apr. 1998.

[20] D. Delbeke, R. Bockstaele, P. Bienstman, R. Baets, and H. Benisty, "High-efficiency semiconductor resonant-cavity light-emitting diodes: A review," *IEEE J. Sel. Topics Quantum Electron.*, vol. 8, no. 2, pp. 189–206, Mar./Apr. 2002.

[21] H. Bensity, R. Stanley, and M. Mayer, "Method of source terms for dipole emission modification in modes of arbitrary planar structures," *J. Opt. Soc. Amer. A*, vol. 15, no. 5, pp. 1192–1201, May 1998.

[22] N. E. J. Hunt, E. F. Schubert, R. A. Logan, and G. J. Zydzik, "Enhanced spectral power density and reduced linewidth at 1.3 μm in an InGaAsP quantum well resonant-cavity light-emitting diode," *Appl. Phys. Lett.*, vol. 61, no. 19, pp. 2287–2289, Nov. 1992.

[23] Y. H. Zhang, H. T. Luo, and W. Z. Shen, "Study on the quantum efficiency of resonant cavity enhanced GaAs far-infrared detectors," *J. Appl. Phys.*, vol. 91, no. 9, pp. 5538–5544, May 2002.

[24] H. T. Luo, Y. H. Zhang, W. Z. Shen, Y. Ding, and G. Yu, "Photon absorption in resonant-cavity-enhanced GaAs far-infrared detectors," *Appl. Opt.*, vol. 41, no. 31, pp. 6537–6542, Nov. 2002.

[25] R. J. Ram, D. I. Babić, R. A. York, and J. E. Bowers, "Spontaneous emission in microcavities with distributed mirrors," *IEEE J. Quantum Electron.*, vol. 31, no. 2, pp. 399–410, Feb. 1995.

[26] H. D. Neve, "Study and Realization of Microcavity Based LED's," Ph.D. dissertation, Dept. Inf. Technol., Univ. Ghent, Ghent, Belgium, 1997.

[27] N. Tsutsui, I. Khmyrova, V. Ryzhii, and T. Ikegami, "Effect of photon recycling in pixelless imaging device," *Jpn. J. Appl. Phys.*, vol. 39, no. 9A, pp. 5080–5082, Sep. 2000.

[28] H. Benisty, H. De Neve, and C. Weisbuch, "Impact of planar microcavity effects on light extraction—Part II: Selected exact simulations and role of photon recycling," *IEEE J. Quantum Electron.*, vol. 34, no. 9, pp. 1632–1643, Sep. 1998.

[29] N. F. Gardner, H. C. Chui, E. I. Chen, M. R. Krames, J.-W. Huang, F. A. Kish, S. A. Stockman, C. P. Kocot, T. S. Tan, and N. Moll, "1.4× efficiency improvement in transparent-substrate $(Al_xGa_{1-x})_{0.5}In_{0.5}P$ light-emitting diodes with thin ($\leqslant 2000$ Å) active regions," *Appl. Phys. Lett.*, vol. 74, no. 15, pp. 2230–2232, Apr. 1999.

L. K. Wu was born in LuoYang, Henan Province, China, on June 4, 1980. He received the B.S. and M.S. degrees in condensed matter physics from Zheng Zhou University, Zheng Zhou, China, in 2001 and 2005, respectively. He is currently working toward the Ph.D. degree in the Department of Physics, Shanghai Jiao Tong University, Shanghai, China.

His main research interests are related to semiconductor device physics.

W. Z. Shen was born in Suzhou, Jiangsu Province, China, on May 22, 1968. He received the Ph.D. degree in semiconductor physics and semiconductor device from Shanghai Institute of Technical Physics, Chinese Academy of Sciences, Beijing, China, in 1995.

From 1995 to 1996, he worked as an Assistant Professor in National Laboratory for Infrared Physics, Shanghai Institute of Technical Physics. From 1996 to 1999, he was a Research Associate in the Department of Physics and Astronomy, Georgia State University, Atlanta. Since 1999, he has been with Shanghai Jiao Tong University, Shnaghai, China, where he is currently a Full Professor in the Department of Physics, and Leader of the Condensed Matter Spectroscopy and Optoelectronic Physics Laboratory. His main research interests are in the fields of optical and electrical properties of semiconductors, as well as semiconductor quantum electronic devices. He has authored and co-authored more than 100 papers.